

Decanethiol as a Corrosion Inhibitor for Carbon Steels Exposed to Aqueous CO₂

Z. Belarbi,^{‡*} J.M. Dominguez Olivo,^{*} F. Farelas,^{*} M. Singer,^{*} D. Young,^{*} and S. Nešić^{*}

Carbon dioxide (CO₂) corrosion mitigation is a challenge in the oil and gas industry. In order to decrease the severity of CO₂ corrosion of carbon steel pipelines and equipment, different mitigation practices are recommended. One such strategy is the application of surface-active chemical inhibitors. The aim of this research was to evaluate the inhibition effectiveness of decanethiol in a CO₂-saturated aqueous electrolyte (1 wt% NaCl). The inhibition properties of decanethiol were evaluated by electrochemical measurements (linear polarization resistance, potentiodynamic sweeps, and electrochemical impedance spectroscopy) and the steel surface was characterized by scanning electron microscopy. The obtained data show that decanethiol can successfully prevent corrosion of carbon steels in a CO₂ environment. An inhibition mechanism was also proposed based on adsorption characteristics and inhibitor film formation.

KEY WORDS: CO₂ corrosion, carbon steel, decanethiol, EIS, surface film

INTRODUCTION

Carbon dioxide (CO₂) corrosion becomes a serious problem when, in the oil and gas industry, significant amounts of CO₂ dissolve in water, causing corrosive degradation of facilities made from carbon steel. One way to minimize internal corrosion of carbon steel pipelines exposed to CO₂ environments is by injecting corrosion inhibitors. Most CO₂ corrosion inhibitors used in the industry are organic compounds containing nitrogen, oxygen, and/or sulfur.¹⁻⁴ The inhibitive action of these chemicals is due to their adsorption at the metal surface.⁵ This process depends upon the metal surface character, the type of aggressive environment, the molecular structure of the inhibitor, and its interaction with the metal surface. In a previous study, Belarbi, et al.,⁶ investigated the role of the potential of zero charge (PZC) and found that the corroding steel surface, relative to this, is positively charged in acidic media; therefore, the adsorption of anions (e.g., ubiquitous Cl⁻) or of inhibitor molecules with a negative structural moiety is favored.

The corrosion resistance of copper immersed in an aqueous solution containing dodecanethiol has been reported.⁷ A dodecanethiol monolayer was determined to retard the reduction of dissolved oxygen and mitigate the growth of copper oxide in sodium chloride (NaCl) solution. In another study, weight-loss measurements showed that similar alkanethiols are able to retard corrosion rates when steel specimens are exposed under top of the line corrosion (TLC) conditions.⁸ Based on the results of these studies, thiols, especially decanethiol and 11-mercaptoundecanoic acid, showed superior mitigation of TLC.⁸ Belarbi, et al.,⁹ investigated the effect of different operating parameters on the inhibition efficacy of decanethiol. The effect of water condensation rate, monoethylene glycol (MEG), hydrogen sulfide (H₂S), and hydrocarbon on inhibitor efficacy was

evaluated. It was found that the presence of MEG, variation of gas temperatures, and water condensation rates did not affect the inhibition efficacy of decanethiol. In sour environments, decanethiol was able to reduce localized corrosion of carbon steel exposed to 30 ppm H₂S. In the presence of a condensable hydrocarbon (heptane), decanethiol lost its inhibition efficacy and showed very poor persistency. However, in the absence of condensable hydrocarbons, decanethiol showed excellent persistency and filming behavior and superior mitigation of TLC.⁸

Despite the large number of corrosion inhibition investigations, minimal research has been reported on the inhibition mechanisms involving thiols, particularly related to the mitigation of carbon steel corrosion. The objective of this study is to advance the understanding of the inhibition mechanism of decanethiol against CO₂ corrosion. A systematic study was performed on X65 mild steel immersed in a NaCl solution saturated with CO₂. By means of linear polarization resistance (LPR) and electrochemical impedance spectroscopy (EIS) measurements and x-ray photoelectron spectroscopy (XPS) surface analysis, the inhibition of mechanism of decanethiol was proposed.

EXPERIMENTAL PROCEDURES

2.1 | Materials and Chemicals

The specimens used for electrochemical measurements were machined from an API 5L X65 mild steel with a tempered martensite microstructure. The chemical composition of this carbon steel is provided in Table 1. The electrolyte was prepared by dissolving NaCl in deionized water, which was then saturated with CO₂. Analytical grade decanethiol, used in this study, was acquired from Sigma-Aldrich.[†]

Submitted for publication: April 5, 2019. Revised and accepted: August 13, 2019. Preprint available online: August 13, 2019, <https://doi.org/10.5006/3233>.

* Corresponding author. E-mail: belarbi@ohio.edu.

[‡] Institute for Corrosion and Multiphase Technology, Department of Chemical and Biomolecular Engineering, Ohio University, Athens, Ohio 45701.

[†] Trade name.

Table 1. Composition (wt%) of API^(A) 5L X65 Mild Steel

Element	C	Nb	Mn	P	S	Ti	V	Ni	Fe
Composition	0.05	0.03	1.51	0.004	<0.001	0.01	0.04	0.04	balance

^(A) American Petroleum Institute (API), 1220 L St. NW, Washington, DC 20005.

2.2 | Electrochemical Measurements

Investigation of the inhibiting properties of decanethiol on mild steel corrosion was performed by electrochemical methods using LPR and EIS. The electrochemical measurements were performed using a three-electrode glass cell configured as shown in Figure 1; key elements are a platinum grid as a counter electrode, Ag/AgCl_{sat} electrode as a reference electrode, X65 mild steel rotating cylinder electrode (RCE) as a working electrode, and an additional rectangular X65 mild steel specimen (surface area = 1 cm²) that was extracted for ex situ XPS analysis. All potentials reported in this paper are referred to an Ag/AgCl_{sat} reference electrode. The reference electrode was linked to the corrosion cell via a Luggin capillary and KCl salt bridge. Prior to each experiment, the RCE was sequentially polished with silicon carbide paper (320, 400, and 600 grit), cleaned with isopropanol in an ultrasonic bath, and air dried before introduction into the cell. The corrosion tests were performed in 1 wt% NaCl at 25°C and 1 bar total pressure (pCO₂ = 0.97 bar). Deoxygenation was achieved by sparging with CO₂ for 2 h; the working electrode was then introduced. The CO₂-saturated solution was maintained at pH 3.8 and was not affected by the injection of decanethiol. To avoid possible noise in electrochemical measurements caused by CO₂ bubbles, the sparge tube was retracted during data acquisition. Purging with CO₂ was continued throughout the test to prevent oxygen contamination and preserve the CO₂-saturated the solution. The rotation speed of the working RCE was set at 1,000 rpm before starting the electrochemical measurements.

The electrochemical measurements were conducted with a Gamry[†] potentiostat/galvanostat. In order to minimize the disturbance of the electrode surface, LPR and EIS data were taken every hour during a total exposure time of 6 h. LPR measurements were performed by polarizing the working electrode from -5 mV to +5 mV from the open-circuit potential (OCP), using a scan rate of 0.125 mV/s. To calculate the instantaneous corrosion rate, the Stern Geary assumptions and a B value of 26 mV were used. The B value for these experiments was taken from previous research conducted on mild steel in a

CO₂ environment.⁶ EIS data were acquired from 10 kHz to 0.1 Hz with seven points per decade and an AC amplitude of 10 mV(rms). EIS scans were analyzed and fit using the software SIMAD[†] (Laboratory Interfaces et Systèmes Electrochimiques -France), which allowed the fitting of both the frequency-dependent analytical expressions and equivalent electrical circuits. Cathodic potentiodynamic polarization sweeps were conducted at the end of the experiment when the corrosion rates were stable, by starting from the OCP up to -1.2 V at a scan rate of 0.125 mV/s. The anodic potentiodynamic sweeps were taken subsequently when the OCP returned to the original value. The anodic sweeps were taken from the OCP up to +400 mV. The ohmic drop was compensated for in all the presented curves.

The full experimental matrix for electrochemical experiments is shown in Table 2. It is important to mention that the concentrations of decanethiol were higher than the solubility limit (2.58 ppm_v at 25°C). Therefore, a layer of the immiscible decanethiol should be present at the top of the liquid phase.

2.3 | Surface Analysis

At the end of each experiment, the steel surface was characterized by a scanning electron microscopy (SEM; JEOL JSM-6090 LV[†]). Imaging was performed at an accelerating voltage of 15 kV using a secondary electron signal (SE). XPS data was acquired with a VG Scientific ESCALAB[†] MKII spectrometer using AlK_α (1,486.6 eV) radiation. The instrumental resolution was 1.2 eV with a slit width of 0.6 cm. XPS analysis was performed at ambient temperature.

RESULTS AND DISCUSSION

3.1 | Linear Polarization Resistance Corrosion Rate

Each experiment started with a freshly polished electrode. The electrode was first allowed to equilibrate at the OCP conditions for 1 h. Then, the first LPR was recorded. The evolution of R_p and the OCP measurements with time for the X65 mild steel specimens, in the absence and in the presence of various concentrations of decanethiol, are displayed in Figure 2. In the absence of decanethiol, the R_p value was approximately 128 Ω·cm² (corrosion rate of 2.7 mm/y; Table 3) and the OCP was -0.68 V_{Ag/AgCl_{sat}}. In the presence of decanethiol, the final R_p decreased to reach a low value of 30 kΩ·cm² (corrosion rate of 0.01 mm/y; Table 3) whereas the OCP shifted to more anodic

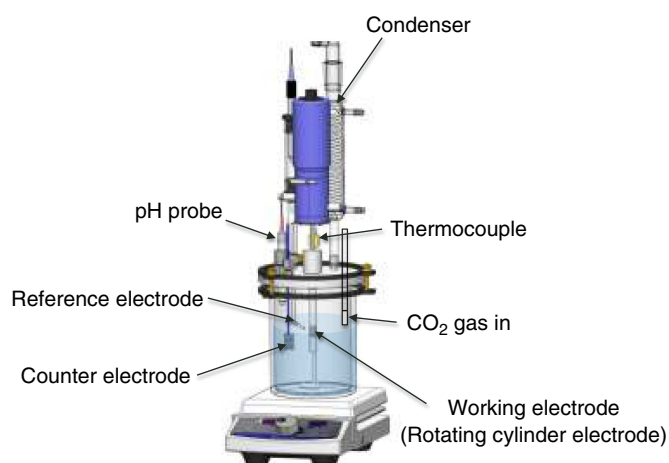


FIGURE 1. Experimental setup for electrochemical tests.⁶

Table 2. Experimental Matrix for Electrochemical Tests	
Total Pressure (bar)	1
pCO ₂ (bar)	0.96
Solution	1 wt% NaCl
Solution temperature	25°C
Working electrode	X65 mild steel
Decanethiol concentration (ppm _v)	0, 5, 10,100, 400
RCE rotation speed (rpm)	1,000

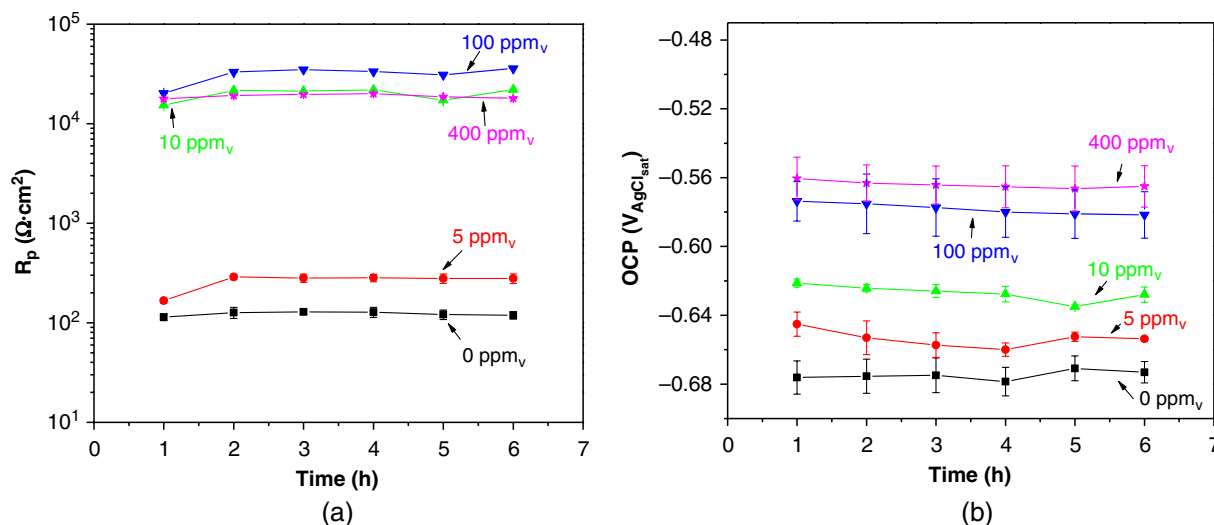


FIGURE 2. R_p as a function of time (a) and OCP (b) of the X65 mild steel immersed in a 1 wt% NaCl solution saturated with CO_2 at 25°C, in the presence and absence of decanethiol.

Table 3. Values of CR at Different Concentration of Decanethiol After 6 h of Immersion

Inhibitor Concentration (ppm)	CR _{LPR} (mm/y)
0	2.70
5	1.07
10	0.02
100	0.01
400	0.02

values. Such an effect could be a result of the retardation in both the anodic and cathodic reactions at the steel surface (caused by adsorption of the inhibitor).

Figure 3 shows the potentiodynamic polarization curves at different thiol concentrations. It can be observed that both cathodic and anodic reactions were retarded by the presence

of thiols. At a first glance, the addition of 5 ppm_v of thiols seemed to retard the anodic reaction more than the cathodic. However, as explained by Dominguez, et al.,¹⁰ this effect is a result of the adsorption of organic corrosion inhibitors only affecting the charge transfer reactions, whereas limiting currents remain unaffected. This behavior results in an increase of the OCP and it is clearly seen with the addition of 10 ppm_v of thiol, as the charge-transfer portion of the cathodic reaction was further retarded whereas the limiting current remained unaffected. After the addition of 100 ppm_v and particularly 400 ppm_v, both reactions were retarded even more.

3.2 | Electrochemical Impedance Spectroscopy

The LPR results were complemented with EIS measurements. Results obtained in a 1 wt% NaCl solution, after 6 h immersion at the corrosion potential (E_{corr}) without and with decanethiol are presented in Figures 4 and 5, respectively. In the absence of inhibitor and at the E_{corr} , the Nyquist diagram (Figures 4[a] and [b]) exhibit single depressed semicircles at high

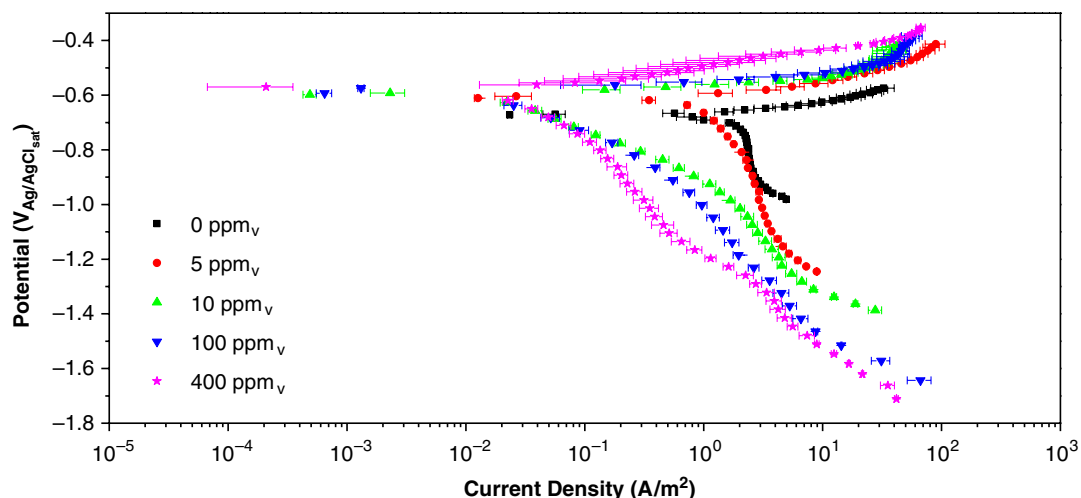


FIGURE 3. Potentiodynamic polarization curve obtained on X65 mild steel immersed in a 1 wt% NaCl solution saturated with CO_2 at 25°C, in the presence and absence of decanethiol.

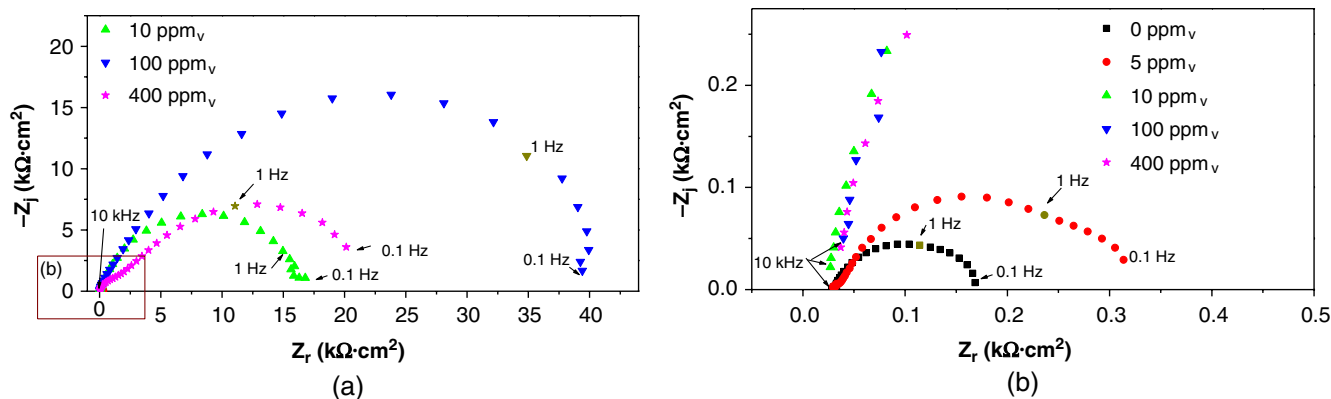


FIGURE 4. (a) Nyquist diagrams of X65 mild steel immersed in a 1 wt% NaCl solution saturated with CO₂ at 25°C, after 6 h in the presence and absence of decanethiol, (b) zoom in at the Nyquist plot at high frequencies (b).

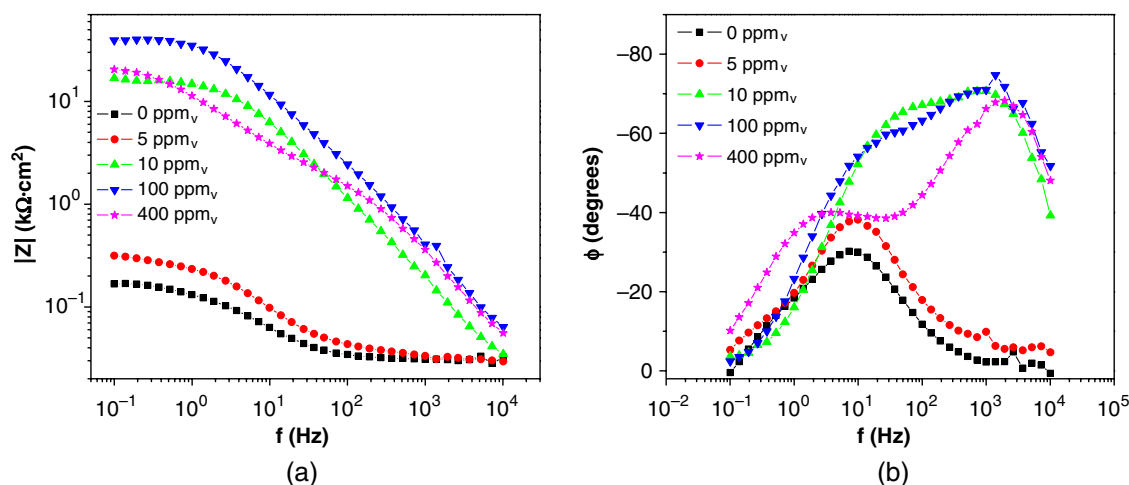


FIGURE 5. Bode diagrams of X65 mild steel immersed in a 1 wt% NaCl solution saturated with CO₂ at 25°C, after 6 h in the presence and absence of decanethiol: (a) modulus; (b) phase.

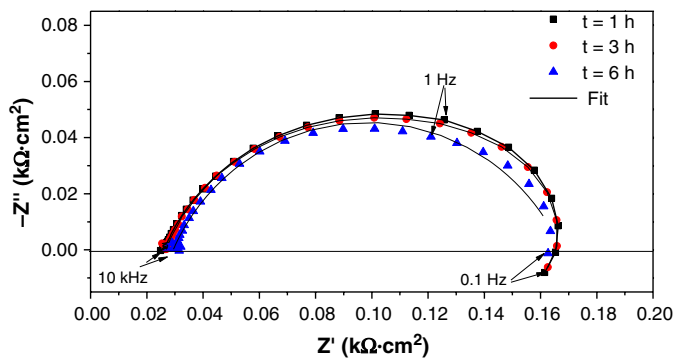
to medium frequencies. Similar results in the absence of corrosion inhibitors have been reported in the literature.^{7-8,11} The high-frequency (HF) capacitive loop is associated to the charge-transfer resistance (R_t) of the corrosion process and the double-layer behavior. The effect of a nonuniform surface (i.e., increased surface roughness) is readily seen by not perfect semicircles.¹² In such cases, the double-layer capacitance (C_{dl}) is replaced by a "constant phase element" (CPE).

In the presence of decanethiol, the low-frequency (LF) limit of the impedance loop increased (Figures 4[a] and [b]), indicating an increase of the polarization resistance. In addition, the impedance modulus value in the inhibited solution (Figure 5[a]) reached a maximum at a concentration of 100 ppm_v, which is higher than measured in the uninhibited solution. Besides the time constant of the charge-transfer process and the double-layer capacitance, a second time constant was observed in the HF domain after adding decanethiol at concentrations higher than 10 ppm_v (Figure 5[b]). This second time constant could be attributed to the adsorbed inhibitor film on the steel surface.

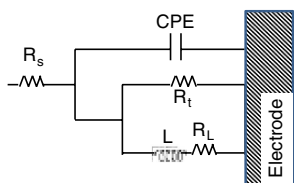
The thickness of the inhibitor layer can be estimated from the EIS measurements by calculating the double-layer capacitance (C_{dl}) and the inhibitor film capacitance (C_f) values. In the absence of inhibitor, the impedance spectra (Figure 6[a]) were fitted to the electrical equivalent circuit presented in Figure 6(b). In CO₂ corrosion of carbon steels, typical EIS diagrams include an HF capacitive loop followed by an inductive

loop at LF.^{6,11,13-16} Belarbi, et al.,¹⁶ have reported an inductive loop at LF range (<0.1 Hz) that may be ascribed to the relaxation process obtained by adsorbed species such as Fe(l)_{ads} and (FeOH)_{ads} on the metal surface. Relaxation is a small rearrangement of the surface layers, which may nevertheless be significant energetically, and seems to be commonplace for metal surfaces. Adsorption of species onto the surface may enhance, alter, or even reverse the process.¹⁷⁻¹⁹ Epelboin and Keddam²⁰ showed that the inductive loop observed at LF could be attributed to partial coverage of the iron surface by an adsorbed intermediate. Almeida, et al.,¹⁵ showed that the capacitive loop associated with the charge-transfer resistance in parallel with the double-layer capacitance. At the mHz frequencies domain, an inductive or capacitive loop can be observed.

The inductive loop was explained by the relaxation of (FeOH)_{ads} adsorbed on the metal surface. Almeida, et al.,¹⁵ developed a better analysis of CO₂ corrosion by calculating the impedance diagrams considering the Langmuir-type adsorption isotherm, in which the fractions of the electrode surface filled by intermediate species Fe(l)_{ads}, (FeOH)_{ads}. The analytical expression of impedance calculated by Almeida, et al.,¹⁵ can be represented by the electric circuit in Figure 5(b). These circuits consist of R_s (the resistance of solution between the working electrode and counter electrode), C_{dl} in parallel to the R_t (charge-transfer resistance), and R_t in parallel with the inductive elements L (inductance) and R_L (inductive resistance).



(a)



(b)

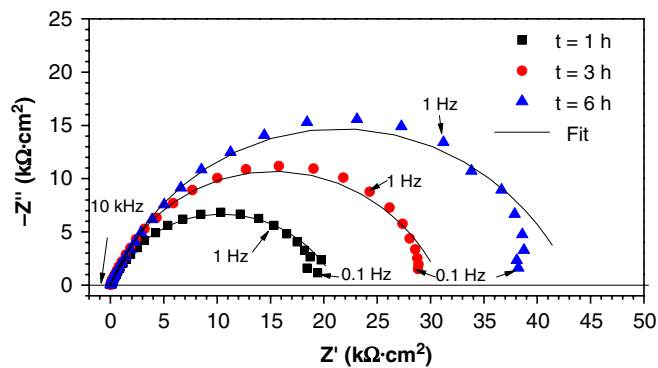
FIGURE 6. Experimental and fitted data of X65 mild steel immersed in 1 wt% NaCl solution in the absence of decanethiol at 25°C (a) and (b) equivalent circuit used for the regression calculation.

In the presence of 100 ppm_v of decanethiol (Figure 7[a]), the LF response and its evolution with immersion time are different from the uninhibited solution. The inductive loop in the LF range disappears. The same behavior was observed at 5 ppm_v, 10 ppm_v, and 400 ppm_v of decanethiol (the impedance diagrams are not presented in this manuscript). This could be a result of the shift of the inductive loop at very low frequencies that we could not see in the range of the studied frequencies. The shift of the inductive loop may be explained by the diminution of the adsorption/desorption processes of intermediate species on the metal surface, resulting from retardation of the cathodic and anodic reactions. In addition to the time constant of the charge-transfer process and the double-layer capacitance, a second-time constant was observed in the HF domain after adding decanethiol at concentrations higher than 10 ppm_v. LPR and potentiodynamic sweeps results suggested that the decanethiol retards the charge-transfer reactions. Therefore, the impedance diagrams obtained at each time and for different concentrations (5 ppm_v, 10 ppm_v, 100 ppm_v, and 400 ppm_v) were fitted to the electrical equivalent circuit presented in Figure 7(b). The time constant in the HF range (order of kHz), R_f C_f, is attributed to inhibitor-film adsorption. C_f and R_f are the capacitance and the resistance associated with the inhibitor film, respectively. The time constant at low frequencies (~10 Hz), R_tC_{dl} is related to the electrochemical reactions at steel surface.

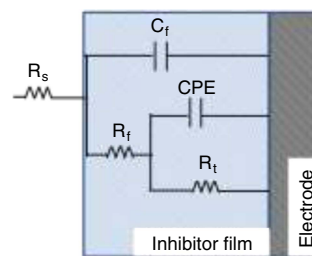
The good agreement between the experimental and fitted data enabled the determination of R_s, Q_{dl}, α, R_t, C_f, and R_f. Brug, et al.,²¹ developed a theory, assuming uniform resistances on the electrode surface and a distributed capacitance, leading to the following equation to calculate the value of C_{dl} as a function of R_s, double-layer CPE coefficient Q_{dl}, and α:

$$C_{dl} = R_s^{(1-\alpha)/\alpha} Q_{dl}^{1/\alpha} \quad (1)$$

Variations of C_{dl}, R_t, C_f, and R_f with immersion time are presented in Figure 8. The solution resistance (R_s) is around



(a)



(b)

FIGURE 7. Experimental and fitted data of X65 mild steel immersed in 1 wt% NaCl solution in presence of 100 ppm_v of decanethiol at 25°C (a) and (b) equivalent circuit used for the regression calculation.

30 Ω·cm². In the absence of decanethiol, the R_t magnitude associated with the charge transfer shows a slight change with time ranging from 158 Ω·cm² to 142 Ω·cm². In the literature,^{11,22-24} it has been postulated that the decrease of R_t stems from the increase of the cementite (Fe₃C) covered surface area, which enhances the galvanic effect associated with Fe₃C, as ferrite oxidatively dissolved. However, the increase of decanethiol concentration generally led to an increase of R_t and decrease of C_{dl}. This is the result of the inhibitor adsorption across the steel surface that retards the charge transfer reactions, thus lowering the corrosion rate. The EIS results were in good agreement with the potentiodynamic polarization curves. In addition, the increase of decanethiol concentration above 10 ppm_v lead to the formation of a self-assembled monolayer (SAM) that will lead to a decrease in C_{dl}. Based on these results, it can be inferred that the threshold concentration for decanethiol in 1 wt% NaCl solution is between 10 ppm_v and 100 ppm_v. However, increasing the concentration of decanethiol above 100 ppm_v did not improve the inhibition efficacy.

The R_t measured with EIS is similar to the one measured by LPR, considering the same measurement frequency.

The thickness of the inhibitor layer can be estimated using the parallel plate model. If the planar condenser model (parallel plate model) is assumed,²⁵ the capacitance (C_f), and the film thickness (d) can be related by Equation (2).²⁵

$$C_f = \epsilon \epsilon_0 / d \quad (2)$$

where ε₀ is the permittivity of the vacuum (9 × 10⁻¹⁴ F/cm), ε is the dielectric constant of inhibitor, and d is the thickness of the inhibitor film. The average value of the dielectric constant for alkanethiolate is around 2.1.²⁶⁻²⁷ If we assume that ε = 2.1, the average calculated thickness "d" of the inhibitor layer from

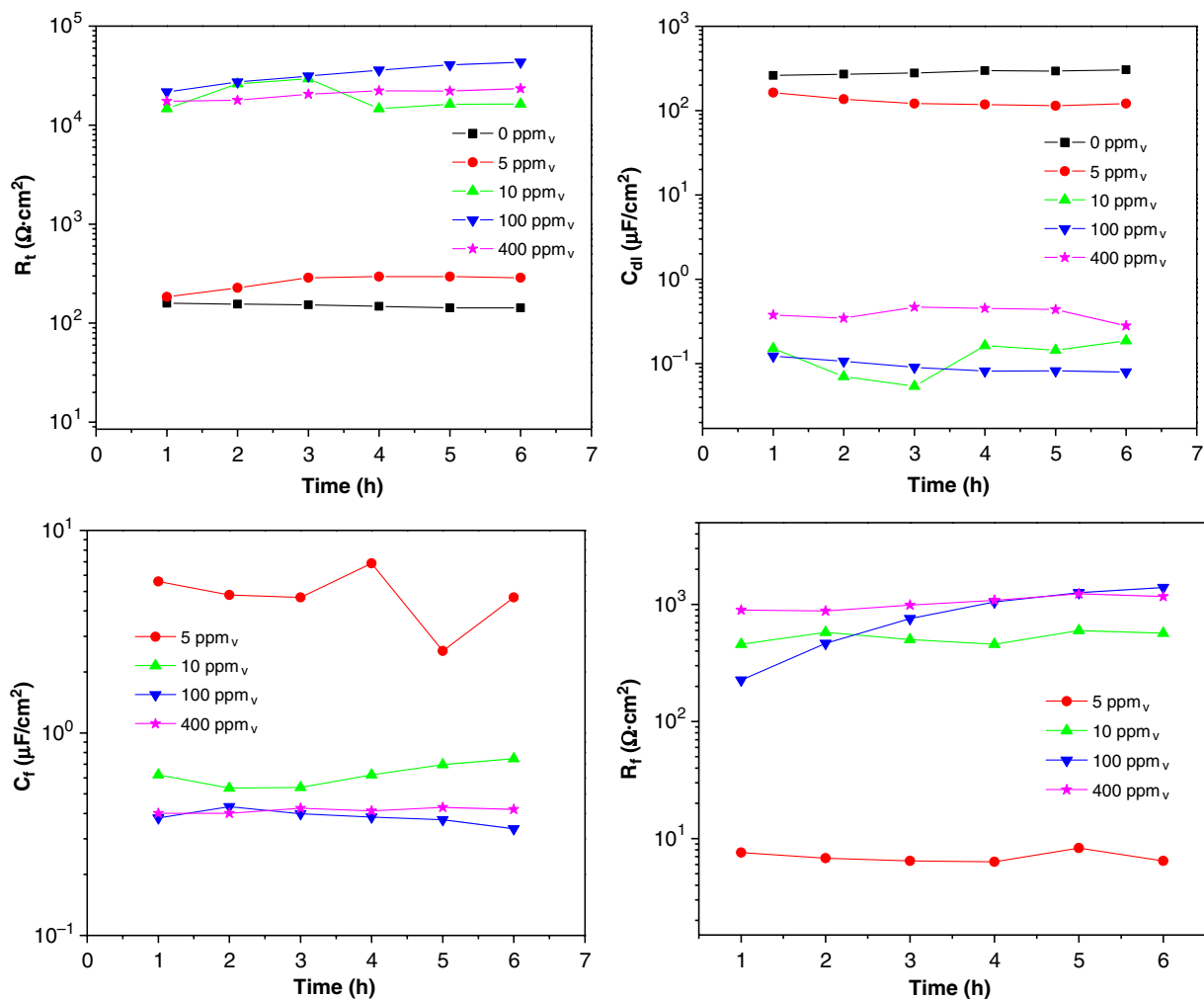


FIGURE 8. Variation of R_t , C_{dl} , C_f and R_f vs. time.

Equation (2) using the C_f (Figure 8) would be 0.4 nm, 3 nm, 5 nm, and 5 nm at 5 ppm_v, 10 ppm_v, 100 ppm_v, and 400 ppm_v, respectively, after exposing carbon steel for 6 h to an inhibited solution (Figure 9). Based on the tail length, obtained for decanethiol and the thickness determined by EIS, the thickness of 3 nm and 5 nm at 10 ppm_v and 100 ppm_v, approximately corresponds to one and two decanethiol molecular lengths, respectively. However, the thickness obtained at 5 ppm_v is lower than a one decanethiol molecular length, which could be the result of randomly organized adsorption (without SAM formation) or due to a tilt angle between the surface and the decanethiol molecules. Based on the result reported in the literature, the formation of a first adsorbed layer is a result of electrostatic interactions between the inhibitor head and the metal surface.⁸ The second layer²⁸⁻²⁹ would be formed with alkyl tails interacting with each other and the hydrophilic group facing the solution.

3.3 | Surface Characterization

3.3.1 | Scanning Electron Microscopy Analysis

Figure 10 shows the SEM images of surface morphological features on the mild steel specimens after electrochemical measurements. It is evident that, without inhibitor, corrosion products formed on the mild steel surface.

In the presence of 5 ppm_v decanethiol, the steel surface was only partially protected. The SEM images show alternating

corroded and protected areas. However, in the presence of decanethiol at 10 ppm_v, 100 ppm_v, and 400 ppm_v, no corrosion was apparent and the polishing marks remained visible after 6 h of exposure to the 1 wt% NaCl electrolyte. The surface of the

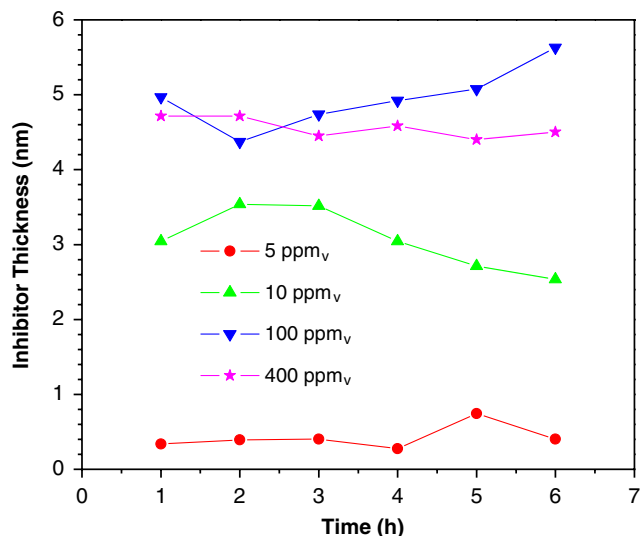


FIGURE 9. Variation of inhibitor thickness vs. time.

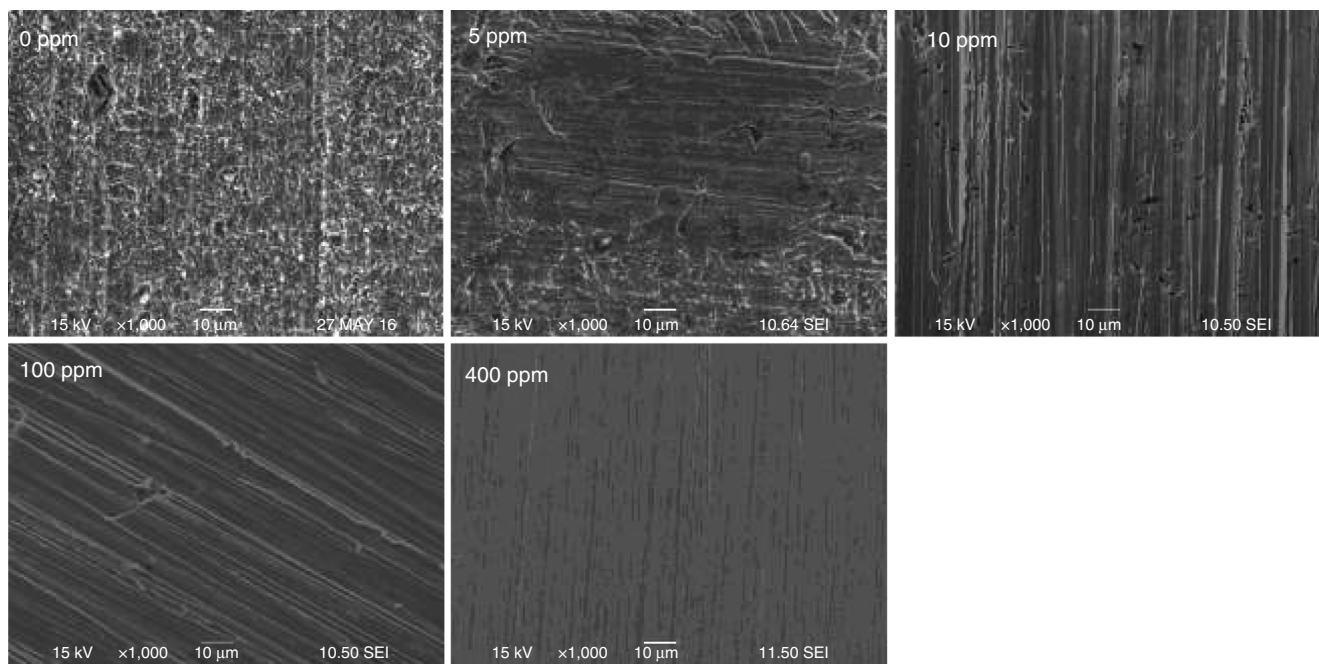


FIGURE 10. Surface morphology of of X65 mild steel immersed in a 1 wt% NaCl solution saturated with CO₂ at 25°C, after 6 h in the presence and absence of decanethiol.

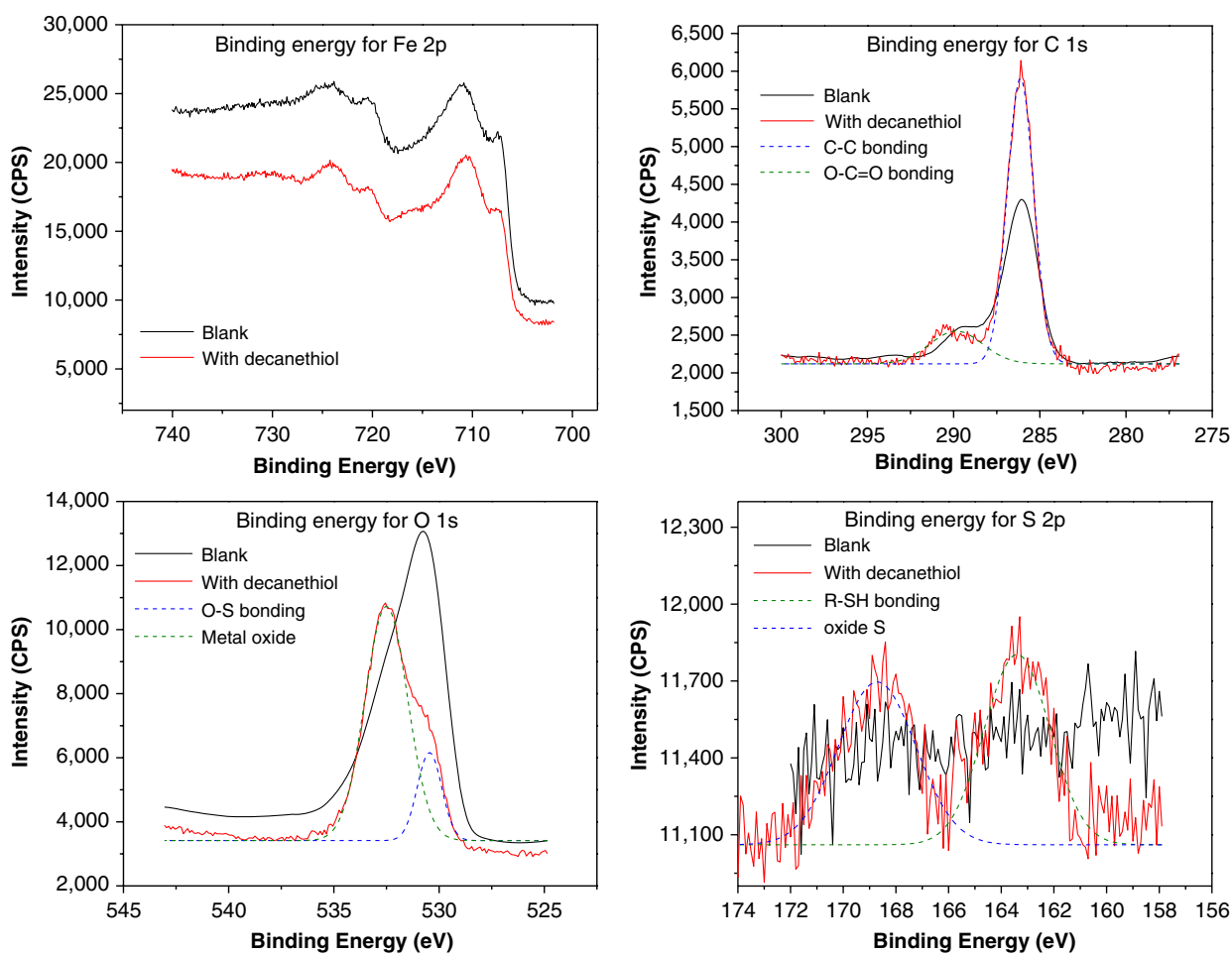


FIGURE 11. XPS spectra of bare steel (blank) and X65 mild steel immersed in a 1 wt% NaCl solution saturated with CO₂ at 25°C, after 6 h in the presence of 400 ppm_v of decanethiol.

mild steel was well-protected. These observations are in good agreement with the electrochemical results.

3.3.2 | X-ray Photoelectron Spectroscopy Analysis

Inhibitor films adsorbed on the steel surface, after 6 h immersion in a 1 wt% NaCl electrolyte in the presence of 400 ppm decanethiol, were characterized by ex situ XPS analysis. High-resolution scans of the Fe 2p, O 1s, C 1s, and S 2p peaks were collected from one spot on each sample using pass energy of 1,486.6 eV to identify the oxidation state of chemical species present on the metal surface.

The results are presented in Figure 11. The recorded spectra for the “blank” reference sample (a freshly polished mild steel) and mild steel treated with decanethiol show a set of peaks characteristic of metallic (Fe) and oxidized iron. Two binding energies of 707.1 eV for Fe 2p_{3/2} and 720.2 eV for Fe 2p_{1/2} were observed, corresponding to Fe 2p of metallic iron.³⁰ The peaks around 710 eV for Fe 2p_{3/2} and 724 eV for Fe 2p_{1/2} correspond to the Fe 2p signatures of oxidized iron species.³¹ The characterization of the inhibitor films adsorbed on the steel surface was completed by the analysis of the O 1s, C 1s, and S 2p spectral regions. The O 1s binding energy spectrum of the bare electrode showed evidence for the presence of oxidized iron species (530.4 eV). In the presence of decanethiol, the O 1s spectrum was deconvoluted into two peaks with binding energies of 530.4 eV and 532 eV, indicating the presence of oxidized iron species and oxidized sulfur (S-O) on the steel surface, respectively. The energy levels of S 2p at 164 eV and 169 eV are compatible with the presence of the free thiol and oxidized sulfur (sulfate or sulfite), respectively. There is no binding energy peak attributable to Fe-S at 162.1 eV, indicating decanethiol is not chemisorbed at the steel surface.³¹ The peak for oxidized sulfur is indicative of oxidation of adsorbed decanethiol upon exposure to air. Baseline XPS data for the bare steel had no peaks attributable to sulfur. The C 1s XPS spectra were fitted by two peaks at 286 eV and 289 eV to 290.5 eV. The peak observed at 286 eV is assigned to carbon atoms of C-C bonds. This peak, which is the result of contamination, is common in XPS and used as an energy reference. It is usually ascribed to oil residues associated with the vacuum system of the spectrometer. Intensity of the 286 eV peak increased in the presence of decanethiol; consequently, observation of C-C bonding can be associated with the presence of an alkyl tail. All these results support the physisorption of decanethiol on the steel surface. Belarbi, et al.,⁸ discussed the possible interactions between the steel surface and thiols.

CONCLUSIONS

The key points of the present study are summarized as follows:

- In situ EIS confirmed the formation of an inhibitor film on the mild steel surface immersed in the CO₂-saturated aqueous solution, resulting in a decrease in corrosion rates as determined by different types of electrochemical measurements (LPR, potentiodynamic sweep).
- The LF impedance response of mild steel at the corrosion potential and its evolution with time of immersion are different with and without inhibitor, showing that the inhibitor clearly influenced the electrochemical process at the steel surface. This analysis shows that the presence of inhibitor decreased the capacitance of the double layer.

- The film thickness was determined for decanethiol using electrochemical impedance spectroscopy and corresponded to a mono- or bi-layer structure.
- XPS characterization was consistent with physisorption of decanethiol on the steel surface; no Fe-S bond formation was detected.

ACKNOWLEDGMENTS

The authors would like to thank the following companies for their financial support: Quadrant Energy, BHP Billiton, BP, Chevron, ConocoPhillips, MI-Swaco, Petronas, PTTEP, Woodside, and Repsol. The authors are grateful to Prof. David Ingram of the “Edwards Accelerator Laboratory—Ohio University” for his help on ex situ XPS experiments. Also, the technical support from the lab’s staff at the Institute for Corrosion and Multiphase Technology by Mr. Alexis Barxias and Mr. Cody Shafer is highly appreciated. The authors are grateful to the “Laboratoire Interfaces et Systèmes Electrochimiques – Pierre and Marie Curie University, France” for the software SIMAD.

References

1. I. Jevremovic, M. Singer, M. Achour, D. Blumer, T. Baugh, V. Miskovic-Stankovic, S. Nešić, *Corrosion* 69, 2 (2013): p. 186-192.
2. R.L. Martin, *Corrosion* 49, 8 (1993): p. 694-701.
3. M. Foss, E. Gulbrandsen, J. Sjöblom, *Corrosion* 64, 12 (2008): p. 905-919.
4. E. Gulbrandsen, A. Granå, *Corrosion* 63, 11 (2007): p. 1009-1020.
5. R. De Marco, W. Durnie, A. Jefferson, B. Kinsella, A. Crawford, *Corrosion* 58, 4 (2002): p. 354-363.
6. Z. Belarbi, F. Farel, M. Singer, S. Nešić, *Corrosion* 72, 10 (2016): p. 1300-1310.
7. Y. Chen, S. Chen, Y. Lei, *Corrosion* 68 (2012): p. 747-753.
8. Z. Belarbi, T.N. Vu, F. Farel, M. Singer, S. Nešić, *Corrosion* 73, 7 (2017): p. 892-899.
9. Z. Belarbi, F. Farel, D. Young, M. Singer, S. Nešić, “Effect of Different Parameters on the Inhibition Efficacy of Decanethiol,” CORROSION 2018, paper no. 10823 (Houston, TX: NACE International, 2018).
10. J.M. Dominguez Olivo, B. Brown, D. Young, S. Nešić, *Corrosion* 75 (2019): p. 137-139.
11. F. Farel, M. Galicia, B. Brown, S. Nešić, H. Castaneda, *Corros. Sci.* 52 (2010): p. 509-517.
12. B. Hirschhorn, M.E. Orazem, B. Tribollet, V. Vivier, I. Frateur, M. Musiani, *J. Electrochem. Soc.* 157, 12 (2010): p. C452-C457.
13. P. Altoe, G. Pimenta, C.F. Moulin, S.L. Diaz, O.R. Mattos, *Electrochim. Acta* 41 (1996): p. 1165-1172.
14. D.S. Carvalho, C.J.B. Joia, O.R. Mattos, *Corros. Sci.* 47 (2005): p. 2974-2986.
15. T. Almeida, M.C.E. Bandeira, R.M. Moreira, O.R. Mattos, *Corros. Sci.* 120 (2017): p. 239-250.
16. Z. Belarbi, B. Brown, M. Singer, S. Nešić, “Study of Adsorption of Corrosion Inhibitor 1-(2-aminoethyl)-2-oleyl-2-imidazolium Chloride on Carbon Steel Under CO₂ Environment by Using In-Situ AFM Measurements,” in CORROSION 2017, paper no. 0990 (Houston, TX: NACE, 2017).
17. P. Zielinski, *Acta Phys. Polon. A* 89 (1996): p. 251-263.
18. J. Sokolov, F. Jona, P.M. Marcus, *Phys. Rev. B* 33 (1986): p. 1397-1400.
19. W.H. Reinmuth, H. Balasubramanian, *Electroanal. Chem. Interf. Electrochem.* 38 (1827): p. 79-94.
20. I. Epelboin, M. Keddam, *J. Electrochem. Soc.* 117 (1970): p. 1052-1056.
21. G.J. Brug, A.G.V.D. Eeden, M. Sluyters-Rehbach, J.H. Sluyters, *J. Electroanal. Chem.* 176 (1984): p. 275-295.
22. D. Staicopolus, *J. Electrochem. Soc.* 110, 11 (1963): p. 1121-1124.
23. K. Videm, *Surf. Sci.* 335 (1995): p. 235-240.
24. S. Al-Hassan, B. Mishra, D. Olson, M. Salama, *Corrosion* 54, 6 (1998): p. 480-491.

25. K. Marušić, H.O. Čurković, H. Takenouti, *Electrochim. Acta* 56 (2011): p. 7491-7502.
26. F.S. Damos, R.C.S. Luz, L.T. Kubota, *Langmuir* 21 (2005): p. 602-609.
27. M.A. Rampi, O.J.A. Schueller, G.M. Whitesides, *Appl. Phys. Lett.* 72, 14 (1998): p. 1781-1783.
28. J.F. Scamehorn, R.S. Schechter, W.H. Wade, *J. Colloid Interf. Sci.* 85 (1982): p. 463-478.
29. M. Knag, K. Bilkova, E. Gulbrandsen, P. Carlsen, J. Sjöblom, *Corros. Sci.* 48 (2006): p. 2592-2613.
30. C. Pirlot, J. Delhalle, J. Pireaux, Z. Mekhalif, *Surf. Coat. Technol.* 138 (2001): p. 166-172.
31. H. Zhang, C. Romero, S. Baldelli, *J. Phys. Chem. B* 109 (2005): p. 15520-15530.